Proceedings of ITC18, 2008

Numerical simulation on the flute instabilities in the GAMMA10 magnetic field

Isao KATANUMA[1)], Katsuya YASHIRO[1)], Tsuyoshi IMAI[1)] and Vladimir P. PASTUKHOV[2)]

[1)] *Plasma Research Center, University of Tsukuba, Tsukuba 305-8577, Japan*

[2)] *RRC "Kurchatov Institute", Kurchatov Square, 1, 123182 Moscow, Russia*

We apply the computer simulation code, which was developed to study the flute modes fluctuation in the divertor, to the GAMMA10 tandem mirror.

Keywords: divertor, flute, interchange, simulation, mirror

1. Introduction

Flute modes are the most dangerous instabilities for open magnetic systems such as GAMMA10 tandem mirror. So that the GAMMA10 contains the non-axisymmetric minimum-B mirror regions for the suppression of the flute instabilities. The non-axisymmetric magnetic field, however, causes the neoclassical radial transport of ions in the central cell, so that the fully axisymmetric tandem mirror is desirable. A divertor magnetic mirror is a candidate for the axisymmetric tandem mirror stable to the flute modes as a future device [1]. There is a plan to replace one of anchor cell in GAMMA10 with an axisymmetric divertor mirror cell [2].

We have derived a set of the basic equations to analyze the flute mode fluctuations in the axisymmetric magnetic divertor and have developed a computer simulation code [3, 4]. In the present paper, we will apply the computer code to the GAMMA10 magnetic field and will perform the computer simulation on the flute mode fluctuations and the associated plasma radial transport.

In order to apply the computer code, where the basic equations used in the code were derived in the axisymmetric systems, to the GAMMA10 with the non-axisymmetric mirror regions, we make the following assumption. The stability criterion of the flute modes is given as [5, 6]

$$\int_{-L}^{L} \frac{(\tilde{p}_\perp + \tilde{p}_\parallel)}{B} \kappa_\psi \mathrm{d}\zeta \geq 0 \qquad (1)$$

Here the anisotropic pressures are written by the separation of variables as $p_\perp(\psi, \zeta) = \tilde{p}_\perp(\zeta)\nu(\psi)$, $p_\parallel(\psi, \zeta) = \tilde{p}_\parallel(\zeta)\nu(\psi)$ and κ_ψ is the normal curvature described in the flux coordinates (ψ, φ, ζ) with $\boldsymbol{B} = \nabla\psi \times \nabla\varphi$,

$$\hat{e}_\parallel \cdot \nabla \hat{e}_\parallel \equiv \boldsymbol{\kappa} = \kappa_\psi \nabla\psi + \kappa_\varphi \nabla\varphi \qquad (2)$$

The familiar stability criterion of the flute modes with isotropic plasma pressure is [7]

$$\delta \int_{-L}^{L} \frac{\mathrm{d}\zeta}{B} < 0 \quad \Rightarrow \quad \frac{\partial U}{\partial \psi} < 0\,, \quad U \equiv \int_{-L}^{L} \frac{\mathrm{d}\zeta}{B} \qquad (3)$$

author's e-mail: katanuma@prc.tsukuba.ac.jp

Noticing that $\partial U/\partial\psi = -2\int \kappa_\psi \mathrm{d}\zeta/B$ in the vacuum magnetic field, where $\nabla_\perp B = B\boldsymbol{\kappa}$, we redefine the specific volume of a magnetic field line U as

$$U = \int_{-L}^{L} \frac{(\tilde{p}_\perp + \tilde{p}_\parallel)}{B} \mathrm{d}\zeta \qquad (4)$$

This definition of specific volume U in eq.(4) satisfies the stability criterion eq.(1) with the axial pressure profile such as in Fig.1. So the simulation code can be applied to the non-axisymmetric magnetic field with anisotropic plasma pressure if the specific volume U defined in eq.(4) is axisymmetric.

2. Application to the GAMMA10 tandem mirror

GAMMA10 is an effectively axisymmetrized tandem mirror, which is designed to satisfy that the integral $\int \kappa_\psi \mathrm{d}\zeta/B$ does not depend on the azimuthal coordinate φ. The definition of U in eq.(4) retains the axisymmetric character of U, and the computer code [3, 4] can be used to calculate the flute mode fluctuations in GAMMA10. The axial plasma pressure profile adopted here is shown in Fig.1.

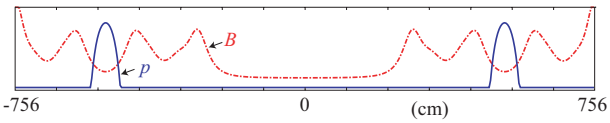

Fig. 1 GAMMA10 axial pressure model. Here $p = \tilde{p}_\perp + \tilde{p}_\parallel$.

Figure 2 plots the radial profiles of the specific volume U for the various ratio $pc \equiv (\tilde{p}_\perp + \tilde{p}_\parallel)_{Anchor}/(\tilde{p}_\perp + \tilde{p}_\parallel)_{central}$. In light of stability criterion eq.(1) or eq.(3), the cases of Figs.2(b) and 2(c) are stable to the flute modes near axis.

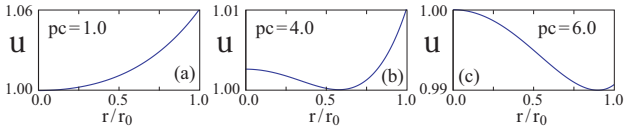

Fig. 2 Radial profiles of $u \equiv U(r)/U(0)$ of GAMMA10.

The basic equations adopted in the code are that the equation of motion of vorticity $\hat{w}$,

$$\partial_t|_\psi \hat{w} + [\![\Phi,\, \hat{w}]\!] - [\![\hat{\rho},\, \langle \frac{v_\alpha^2}{2} \rangle]\!] + \frac{1}{U^\gamma}\frac{\partial U}{\partial \psi}\frac{\partial(\hat{\rho}_0\tilde{T} + \hat{T}_0\tilde{\rho})}{\partial \varphi} = \{DT\}_w \qquad (5)$$

where $\hat{w}$ is related to the specific volume integrated vorticity $\nabla \times (\hat{\rho}\boldsymbol{B} \times \nabla\Phi/B^2)$ due to plasma $\boldsymbol{E} \times \boldsymbol{B}$ drift flux, i.e.

$\hat{w} = wU$. The transport equation of density $\hat{\rho}$ integrated along a magnetic field line, i.e. $\hat{\rho} = \rho U$, is

$$\partial_t|_\psi \hat{\rho} + [\![\Phi, \hat{\rho}]\!] = \{DT\}_\rho \tag{6}$$

And the transport equation of heat $\hat{T}$ integrated along a magnetic field line, i.e. $\hat{T} = TU^{\gamma-1}$, is

$$\partial_t|_\psi \hat{T} + [\![\Phi, \hat{T}]\!] = \{DT\}_T \tag{7}$$

Here the terms $\{DT\}_{w,\rho,T}$ are the classical dissipative terms [3, 4, 8], and $[\![\Phi, \hat{w}]\!] \equiv (\partial\Phi/\partial\psi)\partial\hat{w}/\partial\varphi - (\partial\Phi/\partial\varphi)\partial\hat{w}/\partial\psi$ is known as the Poisson bracket. The quantities with subscript 0 means the equilibrium ones and γ is the adiabatic index $\gamma = 5/3$. The symbol $\langle v_\alpha^2 \rangle$ is the square of plasma flow velocity, and the vorticity $\hat{w}$ can be represented by the scalar potential Φ as

$$\hat{w} = \partial_\psi(\hat{\rho}\langle r^2\rangle\partial_\psi\Phi) + \partial_\varphi\left(\hat{\rho}\langle 1/r^2B^2 + \lambda^2B^2\rangle\partial_\varphi\Phi\right) \tag{8}$$

where $\langle A \rangle$ means the average of A along a magnetic field line.

The linear dispersion relation obtained from eqs.(5)-(8) is

$$\begin{aligned}&(\omega - m\partial_\psi\Phi_0)^2 m^2\hat{\rho}_0\langle 1/r^2B^2 + \lambda^2B^2\rangle \\ &+ (\omega - m\partial_\psi\Phi_0)\left(m(\partial_\psi\hat{\rho}_0)\partial_\psi(\langle r^2\rangle\partial_\psi\Phi_0) - m\partial_\psi\hat{w}_0\right) \\ &- \left((m^2/2)(\partial_\psi\overline{\langle v_\alpha^2\rangle})\partial_\psi\hat{\rho}_0 + (m^2/U^\gamma)(\partial_\psi U)\partial_\psi(\hat{\rho}_0\hat{T}_0)\right) = 0\end{aligned} \tag{9}$$

Here m is the azimuthal mode number and ω is the frequency of the mode. In the case of $\partial_\psi\hat{w}_0 = 0$ and $\partial_\psi\hat{\rho}_0 = 0$, eq.(9) gives the simple dispersion relation of

$$\omega = m\partial_\psi\Phi_0 + \left((1/U^\gamma)(\partial_\psi U)(\partial_\psi\hat{T}_0)/\langle 1/r^2B^2 + \lambda^2B^2\rangle\right)^{1/2} \tag{10}$$

Equation (10) indicates that the mode drifts azimuthally with the $\boldsymbol{E}\times\boldsymbol{B}$ drift velocity, and is unstable if $(\partial_\psi U)\partial_\psi\hat{T}_0 < 0$ which is just the same as the stability condition of flute modes of eqs.(1) or (3).

3. Motivation of the simulation and flute instability

The GAMMA10 tandem mirror improves the axial ion confinement with the help of plug potential formation in the end-mirror cells. Figure 3 is a copy of Fig.6 in [9] as it was. The authors discussed the effects of Neutral beam injection (NBI) on the line densities measured in GAMMA10 in their article [9]. But we are interested in the behavior of the diamagnetism ($\mathsf{DM_{cc}}$) in Fig.3(c) around Time $\simeq$ 130ms. The figure indicates that the diamagnetism dropped suddenly just when the plug ECRH was turned on. We suppose the mechanism of the sudden drop of $\mathsf{DM_{cc}}$ to be the flute mode fluctuations, and carry out the numerical simulation on the flute mode fluctuations.

What kind of effects does the plug-ECRH bring into the GAMMA10 confinement region? It is reasonable to understand that the plug ECRH brings the charge density perturbation into the system, because the plug-ECRH is expected to create the plug potential. The potential, however, is created by the vortex within the framework of MHD as

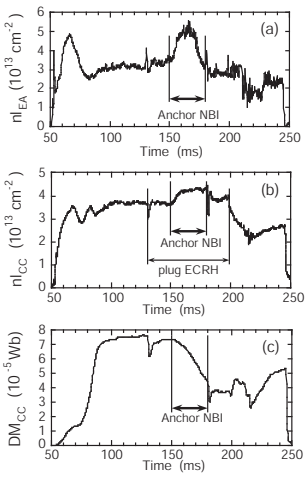

Fig. 3 Time evolution of (a) east anchor line density, (b) central cell line density, and (c) central cell diamagnetism. This figure and the caption are a copy of Fig.6 in [9].

shown in eq.(8), so that the plug ECRH is assumed to bring the vortex into the system.

At first we carry out the simulation in the case of $pc = 1.0$, where the axial pressure is constant and so the specific volume U is Fig.2(a). The flute modes are unstable because of $\partial U/\partial\psi > 0$. The initial condition is that $\hat{w}(x,\varphi) = +1$, $\hat{\rho}(x,\varphi) = 1$, $\hat{T}(x,\varphi) = \exp\{-2x^2\}u^{2/3}$, where all quantities are normalized, and the radial profile of temperature is $T(x,\varphi) = \hat{T}(x,\varphi)/u^{2/3}$. Here $x \equiv r/r_0$, where $r_0 = 18$cm is chosen as the radial position of a limiter. The constant $\hat{w}$ gives the rigid azimuthal rotation of plasma by $\boldsymbol{E}\times\boldsymbol{B}$.

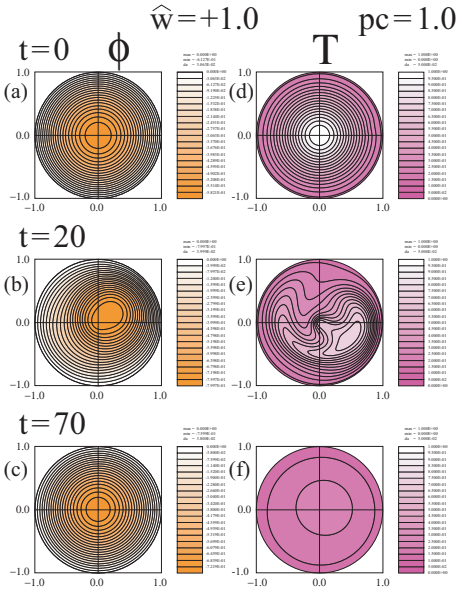

Fig. 4 Contour plots of potential Φ and temperature T at $t = 0$ in (a), (d), at $t = 20$ in (b), (e) and at $t = 70$ in (c), (f). Here each $\Phi(x,\varphi)$ is normalized by its maximum value at each time, while each $T(x,\varphi)$ is normalized by its maximum value at $t = 0$.

Figures 4(a) and 4(d) plot the contour surfaces of the initial potential Φ and initial temperature T profiles, where a small initial perturbation is added to $T(x)$ which is too small to be seen in Fig.4(d). It can be seen that the flute

instability makes the temperature profile flat at $t = 70$.

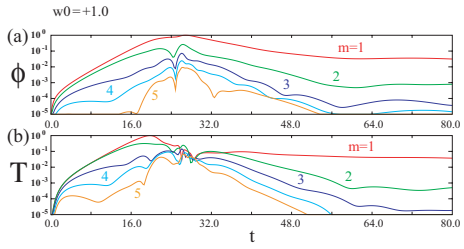

Fig. 5 Time evolution of Fourier components of Φ and T for various azimuthal mode numbers m at $x = 1/2$.

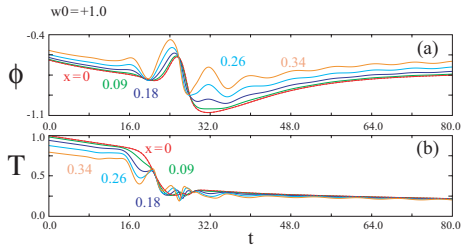

Fig. 6 The time variation of magnitudes of $T(x, \varphi)$ and $\Phi(x, \varphi)$ is plotted as a function of t at $x = 0,\ 0.09,\ 0.18,\ 0.26,\ 0.34$. All data points are at $\varphi = 0$.

Figures 5 shows the time evolution of Fourier components of Φ and T at $x = 1/2$ and Fig.6 plots the time evolution of Φ and T at various x and $\varphi = 0$. Before the flute instability saturates, a large transport of T occurs in Fig.6(b), when the potential profile deviates from the axisymmetry in Fig.4(b). The flute instability saturates when the temperature profile becomes flat radially like Fig.4(f).

4. Effects of the anisotropic potential

The flute instability causes a large energy transport due to the anisotropic potential profile generated by the instability shown in Fig.4(b). If the external μ-wave for plug potential formation (ECRH) brings the perturbed vorticity in the system, the resultant anisotropic potential can cause a large transport just like the flute instability. To investigate this mechanism of transport we carry out the numerical simulation with initial conditions of non-uniform vorticity $\hat{w}$ in Fig.7.

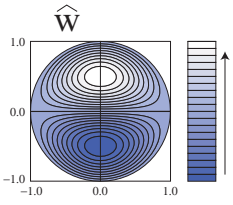

Fig. 7 Initial condition of $\hat{w}(x, \varphi)$.

The initial condition of $\hat{w}$ in Fig.7 is given by

$$\hat{w}(x, \varphi) = w_0 + w_f \sin\{\pi x\} \sin\varphi \qquad (11)$$

Here w_0 and w_f are constants which give the initial potential $\Phi(x, \varphi)$ as shown in Fig.8. The following simulation adopts $pc = 4.0$, that is the radial profile of U is given by Fig.2(b). By changing the coefficients w_0 and w_f, various anisotropic initial potential profile is realized in Fig.8.

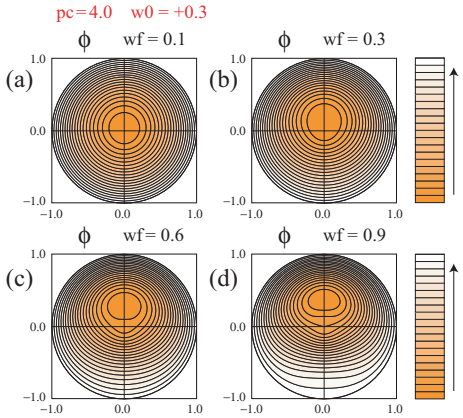

Fig. 8 Initial condition of potential, which is obtained by eqs.(8) and (11) for various w_f. Here the case $w_0 = +0.3$ is plotted.

We show the simulation results of $w_f = 0.1,\ 0.3,\ 0.6,\ 0.9$ with $w_0 = +0.3$. Figures 9–12 plot the time variation of potential $\Phi(x, \varphi = 0)$ and temperature $T(x, \varphi = 0)$ at $x = 0,\ 0.09,\ 0.18,\ 0.26,\ 0.34$, respectively. The temperature T at each local spatial point decreases slowly in time in Figs.9 and 10.

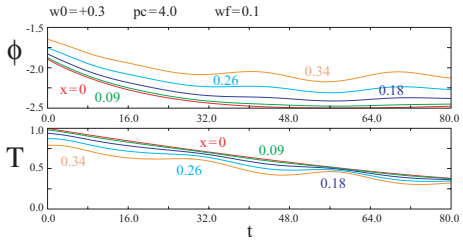

Fig. 9 The time evolution of the potential Φ and T measured at the same positions as Fig.6 for the case of $w_f = 0.1$.

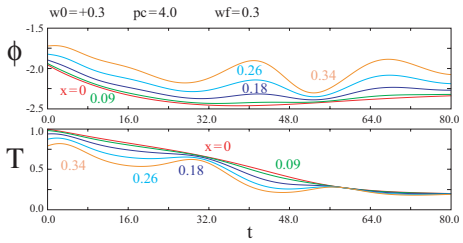

Fig. 10 The time evolution of the potential Φ and T measured at the same positions as Fig.6 for the case of $w_f = 0.3$.

However, a large transport results from the initial anisotropic potential in Figs.11 and 12. After $t = 40$ in Fig.11 and after $t = 30$ in Fig.12 the temperature radial profiles becomes almost flat. So the initial anisotropy of potential has the strong influence on the transport. The oscillations of potential observed in Figs.9–12 comes from the anisotropy of the potential, which means that the initial anisotropy of potential survives for a long time. This can be seen clearly in Fig.13.

Figure 13 plots the time evolution of Fourier amplitudes of potential. The dominant mode is $m = 1$, amplitude of which is order of magnitude larger than other modes $m \neq 1$. The system is not unstable to the flute modes, be-

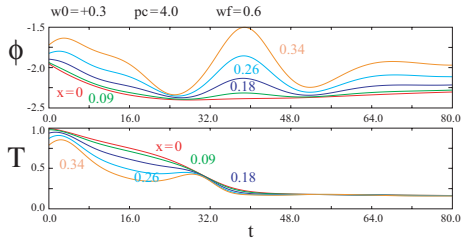

Fig. 11 The time evolution of the potential Φ and T measured at the same positions as Fig.6 for the case of $w_f = 0.6$.

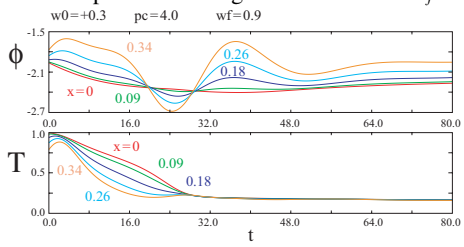

Fig. 12 The time evolution of the potential Φ and T measured at the same positions as Fig.6 for the case of $w_f = 0.9$.

cause the $m = 1$ initial perturbation of Φ does not grows in time, but the system is in the marginally stable state.

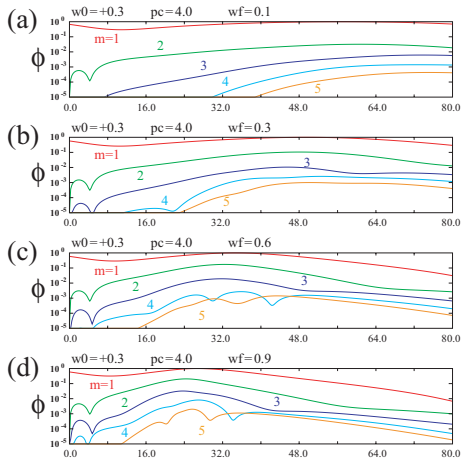

Fig. 13 The time evolution of Fourier amplitudes $m = 1 \sim 5$ for $w_0 = 0.3$.

The cases of high potential of $w_0 = +3.0$ are plotted in Figs.14, 15. The anisotropy of initial potential is given by the ratio w_f/w_0 only. The comparison of two cases $w_0 = +0.3$ and $w_0 = +3.0$ indicates that a larger magnitude of potential cause larger transport as long as the ratio w_f/w_0 is the same. This results is supported by the consideration that the transport results from the $\boldsymbol{E} \times \boldsymbol{B}$-drifts, that is the larger magnitude $\boldsymbol{E}$ cause the larger magnitude of drifts.

The time evolution of Fourier amplitude of potential Φ in the case $w_0 = +3.0$ is plotted in Fig.16. The $m = 1$ initial perturbation of Φ is the dominant mode in this case, and which decreases in time so that the system is stable.

5. Summary

We applied the simulation code, which developed for the axisymmetric system, to the non-axisymmetric tandem mirror, taking into account the effect of axial pressure profile to the magnetic specific volume U. In the case of the

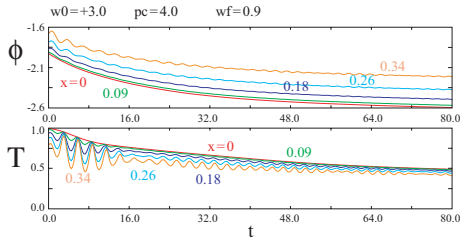

Fig. 14 The time evolution of the potential Φ and T measured at the same positions as Fig.6 for the case of $w_0 = 3.0$ and $w_f = 0.9$.

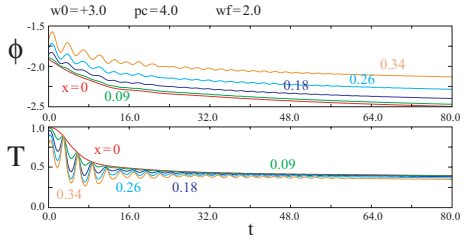

Fig. 15 The time evolution of the potential Φ and T measured at the same positions as Fig.6 for the case of $w_0 = 3.0$ and $w_f = 2.0$.

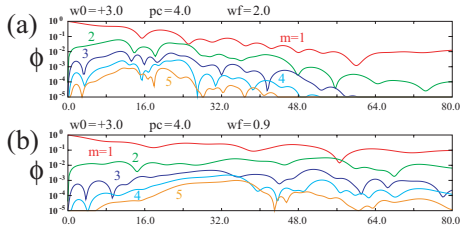

Fig. 16 The time evolution of Fourier amplitudes $m = 1 \sim 5$ for $w_0 = 3.0$.

uniform axial pressure profile, the system was unstable to the flute modes which caused a large energy transport.

The initial anisotropy of potential, which is realized by the initial anisotropic vorticity $\hat{w}$, causes a large energy transport even in the system stable to the flute modes. The mechanism of transport comes from the $\boldsymbol{E} \times \boldsymbol{B}$-drift in the radial direction due to the flute-like fluctuations having a long life time. The life time of this flute-like fluctuations becomes shorter in a very stable state to the flute modes in Fig.2(c) than that in Fig.2(b)

[1] I.Katanuma, Y.Sasagawa, Y.Tatematsu, Y.Nakashima, T.Cho, V.P.Pastukhov; Nucl. Fusion, **46**, 608(2006).
[2] I.Katanuma, H.Saimaru, Y.Mizoguchi, K.Yashiro, T.Cho, V.P.Pastuhkov; Trans. Fus. Sci. Tech. **51**, 122(2007).
[3] I.Katanuma, V.P.Pastukhov, T.Imai, M.Ichimura, T.Kariya et al.; J. Plas. Fus. Res. **84**, 279(2008).
[4] I.Katanuma, et al.; J. Plas. Fus. Res. **84**, 279(2008).
[5] *Physics Basis for MFTF-B, ed. D.E.Boldwin, B.G.Logan, T.C.Simonen; UCID-18496-Part 2 (1980).*
[6] I.Katanuma, T.Tatematsu, K.Ishii, T.Saito and K.Yatsu; J. Phys. Soc.Jpn. **69**, 3244(2000).
[7] M.N.Rosenbluth and C.L.Longmire, Ann. Phys. **1**, 120(1957).
[8] S.I.Braginskiin *Reviews of Plasma Physics*, ed. A.M.A.Leontovich (Consultants Bureau, New York, 1965) Vol. 1.
[9] K.Yatsu, et.al.; Nucl. Fusion, **41**, 613(2001).